2

Electromagnet analysis

2.1 Introduction

The characteristic behaviour of the electromagnets used to suspend the experimental research vehicle must be analysed and modelled before an electromagnet control law can be synthesised. The behaviour of suspension electromagnets is complicated by their nonlinear and unstable nature, and the dynamic geometry changes associated with the electromagnet moving along an uneven track.

Kortüm and Utzt[31] have shown that a linearised model of a suspension electromagnet is inadequate for effective simulation of the full operational envelope of a suspension electromagnet. This chapter therefore presents a detailed nonlinear analysis and a set of model equations which give good accuracy over the full operational envelope of the experimental electromagnets.

The geometry and specification of the experimental electromagnet are outlined first. Then the steady-state behaviour of the electromagnet is modelled. This is followed by modelling of the dynamic behaviour of the electromagnet flux. The chapter is concluded with a summary of the electromagnet model equations and their accuracy.

2.2 Electromagnet geometry and specification

Figure 2.1 shows the physical arrangement of the experimental U-shaped electromagnet and the inverted U-shaped track. Magnetic flux passes through the air gap between the poles of the electromagnet and track and this generates a force of attraction which suspends the electromagnet beneath the track.

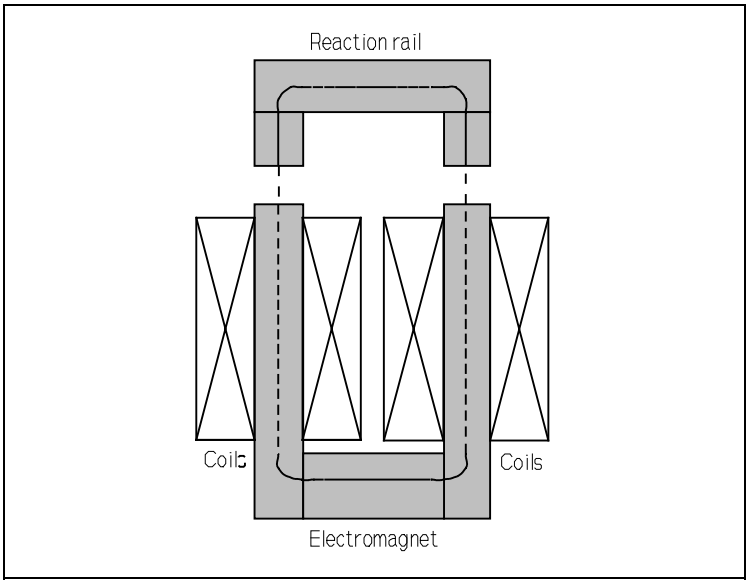

Figure 2.1 Physical arrangement of the electromagnet and track (cross-section perpendicular to track axis)

The electromagnets used for this research were previously used on a research vehicle at the University of Warwick.[32,33] They consist of insulated copper windings wound on steel cores and were designed to lift a maximum load of 50 kg at a nominal operating air gap of 3-4 mm. Table 2.1 lists the electromagnet dimension indices along with the relevant values for the experimental electromagnet.

2.3 Steady-state analysis

The role of an electromagnet in a vehicle suspension application is that of a controlled force actuator. Excitation of the electromagnet coils generates a magneto-motive force which causes a magnetic flux to flow through the electromagnet, air gaps and track. The interaction of the air gap flux and field strength generates a force of attraction between the electromagnet and the reaction rail. The steady-state force characteristic of the experimental electromagnet will now be analysed and model equations developed. The analysis is performed by considering the following:

- fundamental magnetic force characteristic.
- lift and lateral force components.
- air gap reluctance.
- iron path reluctance.
- leakage path reluctance.

Table 2.1 Experimental electromagnet dimension indices and values

Index	Value	Dimension
l	200 mm	Length of the electromagnet
w	33 mm	Width between the electromagnet pole pieces
h	63 mm	Height of the pole pieces above the yoke
p	9.5 mm	Width of the pole pieces
t	30 mm	Width between the track pole pieces
g	0-7 mm	Suspension air gap length
N	274 turns	Total number of coils
R_{coils}	0.8 Ω	Resistance of the coils
ρ	100 nΩm	Resistivity of the steel cores (estimated value)
m	7.3 kg	Mass of the electromagnet

2.3.1 Magnetic force characteristic

By assuming that the poles of the electromagnet and the track have equal magnetic potential over their working faces, the force of attraction across each air gap, F_{airgap}, between the electromagnet and track is given by:[34]

$$F_{airgap} = \frac{1}{2} H_{airgap} \Phi_{airgap} \qquad newtons \qquad \textbf{2.1}$$

where H_{airgap} is the magneto-motive force gradient across each air gap and Φ_{airgap} is the air gap magnetic flux. As force is generated across two air gaps, the total electromagnet lift force, F_{magnet}, is given by:

$$F_{magnet} = 2 F_{airgap} = H_{airgap} \Phi_{airgap} \qquad newtons \qquad \textbf{2.2}$$

Equation 2.2 can be more conveniently expressed by considering it in terms of the magneto-motive force across each air gap, M_{airgap}, and the reluctance of each air gap, R_{airgap}.

The magneto-motive force gradient and air gap flux can be expressed as:

$$H_{airgap} = \frac{M_{airgap}}{g} \qquad amperes/metre \qquad \textbf{2.3}$$

$$\Phi_{airgap} = \frac{M_{airgap}}{R_{airgap}} \qquad webers \qquad \textbf{2.4}$$

where g is the length of each air gap. Substituting Equations 2.3 and 2.4 into Equation 2.2 gives:

$$F_{magnet} = \frac{M_{airgap}^2}{g\,R_{airgap}} \qquad newtons \qquad \textbf{2.5}$$

A first order approximation for the electromagnet lift force may be made by assuming the iron paths to have zero reluctance (i.e. infinite permeability), and that the air gap flux density between the poles, is uniformly distributed over an area equal to the pole face area. This gives the first order approximations for the air gap magneto-motive force, M'_{airgap}, and reluctance, R'_{airgap}, as:

$$M'_{airgap} = \frac{NI}{2} \qquad amperes \qquad \textbf{2.6}$$

$$R'_{airgap} = \frac{g}{\mu_o A_{pole}} \qquad amperes/weber \qquad \textbf{2.7}$$

where N is the total number of coil turns, I is the current flowing through the coils, μ_o is the permeability of free space and A_{pole} is the pole face area. These two expressions may be substituted into Equation 2.5 to give a first order approximation for the lift force, F'_{magnet}, as:

$$F'_{magnet} = \frac{\mu_o (NI)^2 A_{pole}}{4 g^2} \qquad newtons \qquad \textbf{2.8}$$

Equation 2.8 shows that the magnetic force is a nonlinear function of both current and air gap length. Also, it shows that for a constant current the force decreases with increasing air gap, hence it has a negative stiffness coefficient. There is therefore no point of equilibrium between two magnetised bodies,[35] and so the open-loop force-air gap characteristic of an electromagnet is unstable. Figure 2.2 shows a graph of the

electromagnet force characteristic predicted by the first order approximation given by Equation 2.8.

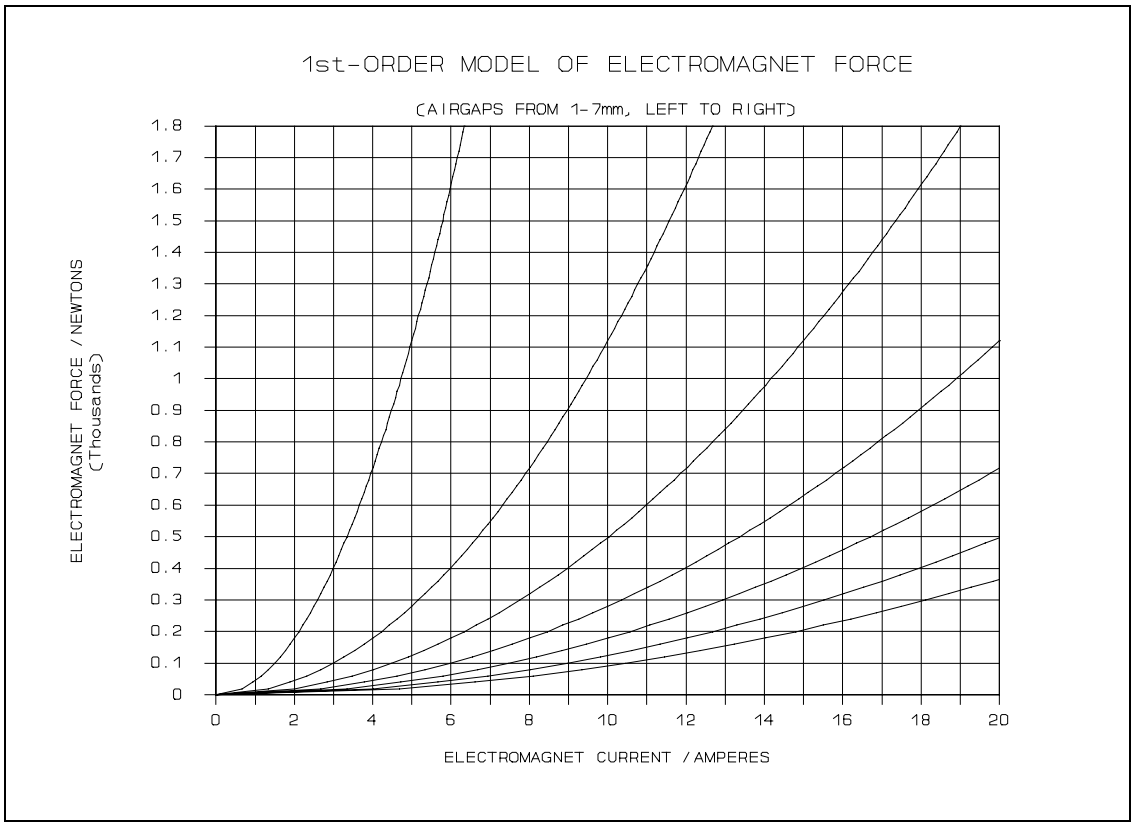

Figure 2.2 First-order model of electromagnet lift force (Equation 2.8)

The assumption of uniform air gap flux distribution is valid only for air gaps that are much smaller than the pole width. At larger air gaps, flux fringing increases the effective air gap flux area and hence decreases the air gap reluctance. Since the first order approximation neglects flux fringing and cannot determine the effects of lateral displacement of the electromagnet relative to the track, a more detailed analysis is required.

2.3.2 Lift and lateral force components

The experimental suspension electromagnet is relatively long and thin. Therefore, end-effects can be neglected and a 2-dimensional analysis can be performed by considering the electromagnet cross-section. This assumption is not strictly true with regard to eddy-currents when the electromagnet is moving along its rail, so they are analysed independently in Section 2.4.4. By assuming the pole surfaces to be magnetic equipotentials, the electromagnet force can be determined using conformal mapping

techniques, but an exact analysis considering all four corners is difficult because the expressions involve complex elliptic integrals and require the solution of implicit equations containing elliptic functions.[36] However, by assuming that an interval of uniform magnetic field exists in the air gap, the problem may be reduced to the sum of 2 two-corner problems, which produce the following simpler formulas for lift and lateral forces:[37]

$$F_{lift} = F'_{magnet}\left[1+\frac{2g}{\pi p}\left(1-\frac{y}{g}\tan^{-1}\frac{y}{g}\right)\right] \qquad newtons \qquad \textbf{2.9}$$

$$F_{lateral} = F'_{magnet}\left[\frac{2g}{\pi p}\tan^{-1}\frac{y}{g}\right] \qquad newtons \qquad \textbf{2.10}$$

where F'_{magnet} is the first order approximation for electromagnet force (Equation 2.8), p is the pole width and y is the lateral offset between the electromagnet and track poles. The uniform magnetic field assumption limits the useful range of these expressions to a maximum air gap and lateral offset of about two-thirds of the pole width.

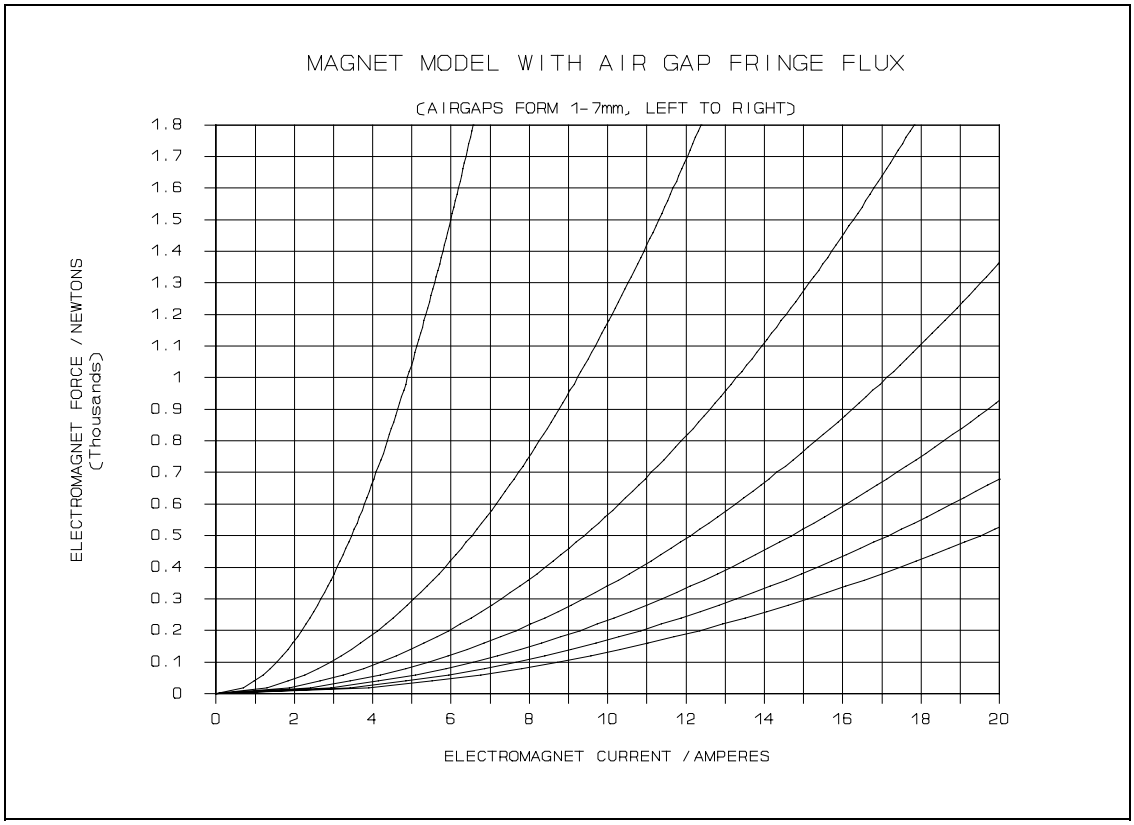

Figure 2.3 Electromagnet lift force model with air gap fringe flux (Equation 2.9)

Figure 2.3 shows a graph of the electromagnet lift force characteristic predicted by Equation 2.9. This graph indicates a maximum increase in force relative to the first

order approximation (Equation 2.8) of 40% at an air gap of 7 mm, falling to a decrease of 7½% at an air gap of 1 mm. The decrease in force at 1 mm is due to the slight difference between the track pole separation and the electromagnet pole separation.

2.3.3 Air gap reluctance

The flux fringing correction factor in Equation 2.9 cannot be applied directly to the air gap reluctance (Equation 2.7) because of the inclusion of the orthogonal force components. However, by considering the case of zero lateral offset, the effects of flux fringing can be modelled simply and to a good degree of accuracy. This does not prejudice the application of the full accuracy model for orthogonal forces later on. The air gap reluctance incorporating lateral fringe flux is given by:

$$R_{airgap} = \frac{g}{\mu_o \, l \left(p + \frac{2g}{\pi} \right)} \qquad \textit{amperes/weber} \qquad \textbf{2.11}$$

Equations 2.9, 2.10 and 2.11 model the lift and lateral force components and the air gap reluctance, but the magneto-motive force across the air gap (Equation 2.6) still neglects the magneto-motive force needed to overcome the reluctance of the iron paths due to their finite permeability.

2.3.4 Iron path reluctance

The reluctance of the iron paths is a function of their geometry and the relative permeability (μ_r) of the core material. Since the permeability is a non-linear function of past and present flux density, incorporating the effects of hysteresis and saturation, it is very difficult to quantify exactly. It is presumably for this reason that most researchers in this field choose to neglect its effect by assuming infinite permeability.

The experimental suspension electromagnets are assumed to be made of mild steel for which the typical maximum permeability is about 2000-3000,[38] and the variation of permeability with flux density[39] is outlined in Table 2.2. To accommodate the fact that the cores of the experimental electromagnet and track have been machined and welded without subsequent heat treatment, a maximum value for μ_r of 2000 has been assumed. With air gaps ranging from about 1% to 7% of the iron path length, the iron

Table 2.2 Typical variation of μ_r for mild steel

Flux density	μ_r / maximum μ_r
0 T	10 %
0.15 T	50 %
0.4 - 1.0 T	100 %
1.3 T	50 %
1.5 T	10 %
2.1 T	$\mu_r = 1$ (saturation)

path reluctance is significant, causing a reduction in force at small air gaps and/or high flux densities.

The reluctance of the track, R_{track}, and electromagnet core, R_{magnet}, are given by:

$$R_{track} = \frac{(t+4p)}{\mu_T \, \mu_o \, lp} \qquad amperes/weber \qquad \textbf{2.12}$$

$$R_{magnet} = \frac{(2h+w+2p)}{\mu_M \, \mu_o \, lp} \qquad amperes/weber \qquad \textbf{2.13}$$

where t is the width between the track poles, w is the width between the electromagnet poles, p is the pole width (and rail pole height), h is the pole height above the yoke, l is the length of the electromagnet and μ_T, μ_M are the relative permeabilities of the track and electromagnet respectively.

Consideration of the iron path reluctance is required to determine the operational limits of the electromagnet (due to the onset of saturation) and also to enable it to be controlled over its full operational envelope. To evaluate the reluctance of the iron paths, the permeability must be known, and this in turn requires knowledge of the flux density. Therefore, the leakage flux between the electromagnet poles must be investigated since the electromagnet core carries both useful suspension flux and the parasitic leakage flux.

2.3.5 Leakage path reluctance

The magneto-motive force between the poles of the electromagnet causes a parasitic leakage flux to flow between them in addition to the useful suspension flux which flows through the air gaps and the track (see Figure 2.4). Finite element analysis has shown that the leakage flux can exceed the suspension flux at large operational air gaps.[40]

The leakage flux path reluctance must therefore be modelled. By assuming the magneto-motive force to be generated linearly over the length of the vertical pole pieces, the effective height of the poles is halved. A first order approximation to leakage flux reluctance can now be made by neglecting fringe flux. This gives:

$$R'_{leakage} = \frac{w}{\mu_o l\left(\frac{h}{2}\right)} \qquad amperes/weber \qquad \textbf{2.14}$$

where w is the width between the poles, l is the length of the electromagnet and h is the height of the poles. Using the expression obtained earlier for the air gap path reluctance (Equation 2.11), the above expression for the leakage reluctance can be modified to include leakage fringe flux at the ends and on top of the electromagnet. This gives:

$$R_{leakage} = \frac{w}{\mu_o\left(l + \frac{2w}{\pi}\right)\left(\frac{h}{2} + \frac{w}{\pi}\right)} \qquad amperes/weber \qquad \textbf{2.15}$$

The incorporation of flux fringing above the top of the electromagnet poles is bound to overestimate the leakage flux at small air gaps due to the close proximity of the track poles and yoke. However, since the effect of leakage flux on the steady-state force is significant only at larger air gaps, this fact is not a problem.

Flux leakage around the outer faces of the electromagnet poles has not been modelled because observation of flux plots obtained using finite element techniques[41] shows that such leakage is not significant for the U-shaped electromagnets.

2.3.6 Steady-state model equations

The model equations for the reluctance of the air gap, leakage and core flux paths are now combined to build model equations for the electromagnet lift and lateral forces.

The magnetic flux paths of the electromagnet and rail are modelled by the equivalent circuit shown in Figure 2.4. The coil windings generate a magneto-motive force, M_{coils}, given by:

$$M_{coils} = NI \qquad amperes \tag{2.16}$$

This drives flux through the electromagnet (reluctance = R_{magnet}), where it splits between the useful path carrying suspension flux (reluctance = $2R_{airgap} + R_{track}$), and a parasitic path carrying leakage flux (reluctance = $R_{leakage}$).

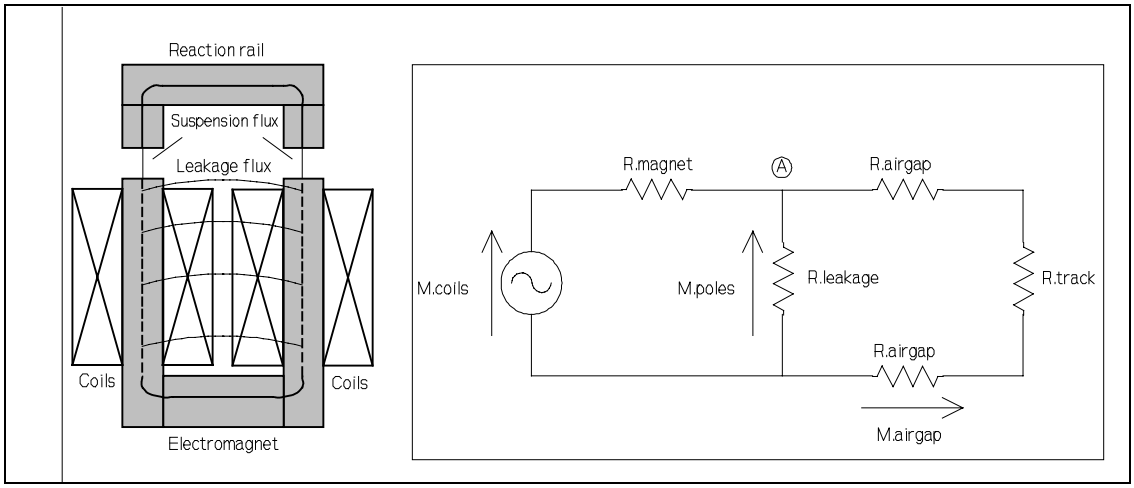

Figure 2.4 Magnet flux paths and flux model circuit diagram

The expression for electromagnet force given in Equation 2.5 is repeated here for convenience:

$$F_{magnet} = \frac{M_{airgap}^2}{g\,R_{airgap}} \qquad newtons \tag{2.17}$$

The above equation requires an expression for M_{airgap} in terms of M_{coils}. Network analysis of the flux circuit diagram is detailed in Appendix A and produces the following result:

$$M_{airgap} = \frac{R_{airgap}R_{leakage}}{(R_{track}+2R_{airgap})(R_{leakage}+R_{magnet})+R_{magnet}R_{leakage}}\,M_{coils} \tag{2.18}$$

Substituting for M_{airgap} (Equation 2.18) into Equation 2.17 gives:

$$F_{magnet} = \frac{R_{airgap} R_{leakage}^2}{g\left[(R_{track} + 2R_{airgap})(R_{leakage} + R_{magnet}) + R_{magnet} R_{leakage}\right]^2} M_{coils}^2 \quad newtons \qquad \textbf{2.19}$$

where R_{airgap}, $R_{leakage}$, R_{track} and R_{magnet} are defined by Equations 2.11, 2.15, 2.12 and 2.13 respectively. The lift and lateral forces can now be expressed by using the factors in Equations 2.9 and 2.10 and compensating these for the fact that the air gap reluctance already incorporates flux fringing at zero lateral offset, this gives:

$$F_{lift} = F_{magnet}\left[1 - \frac{y/g \ \tan^{-1} y/g}{1 + \pi p/2g}\right] \quad newtons \qquad \textbf{2.20}$$

$$F_{lateral} = F_{magnet}\left[\frac{\tan^{-1} y/g}{1 + \pi p/2g}\right] \quad newtons \qquad \textbf{2.21}$$

These equations are needed to model the difference between the pole spacings of the electromagnet and track in addition to modelling lateral offsets between the track and the electromagnet.

An expression for the air gap flux can now be obtained by substituting for M_{airgap} (Equation 2.18) into Equation 2.4 giving:

$$\Phi_{airgap} = \frac{R_{leakage}}{(R_{track} + 2R_{airgap})(R_{leakage} + R_{magnet}) + R_{magnet} R_{leakage}} M_{coils} \quad webers \qquad \textbf{2.22}$$

An expression for the leakage flux is obtained similarly giving:

$$\Phi_{leakage} = \frac{R_{track} + 2R_{airgap}}{(R_{track} + 2R_{airgap})(R_{leakage} + R_{magnet}) + R_{magnet} R_{leakage}} M_{coils} \quad webers \qquad \textbf{2.23}$$

The flux which flows through the yoke of the electromagnet is the sum of the air gap and leakage fluxes above, giving:

$$\Phi_{magnet} = \frac{R_{track} + 2R_{airgap} + R_{leakage}}{(R_{track} + 2R_{airgap})(R_{leakage} + R_{magnet}) + R_{magnet} R_{leakage}} M_{coils} \quad webers \qquad \textbf{2.24}$$

Figure 2.5 shows a graph of the electromagnet lift force characteristic given by Equation 2.20 with a fixed value for the permeability of the iron paths. This graph predicts a decrease in lift force relative to the previous graph (Figure 2.3) of

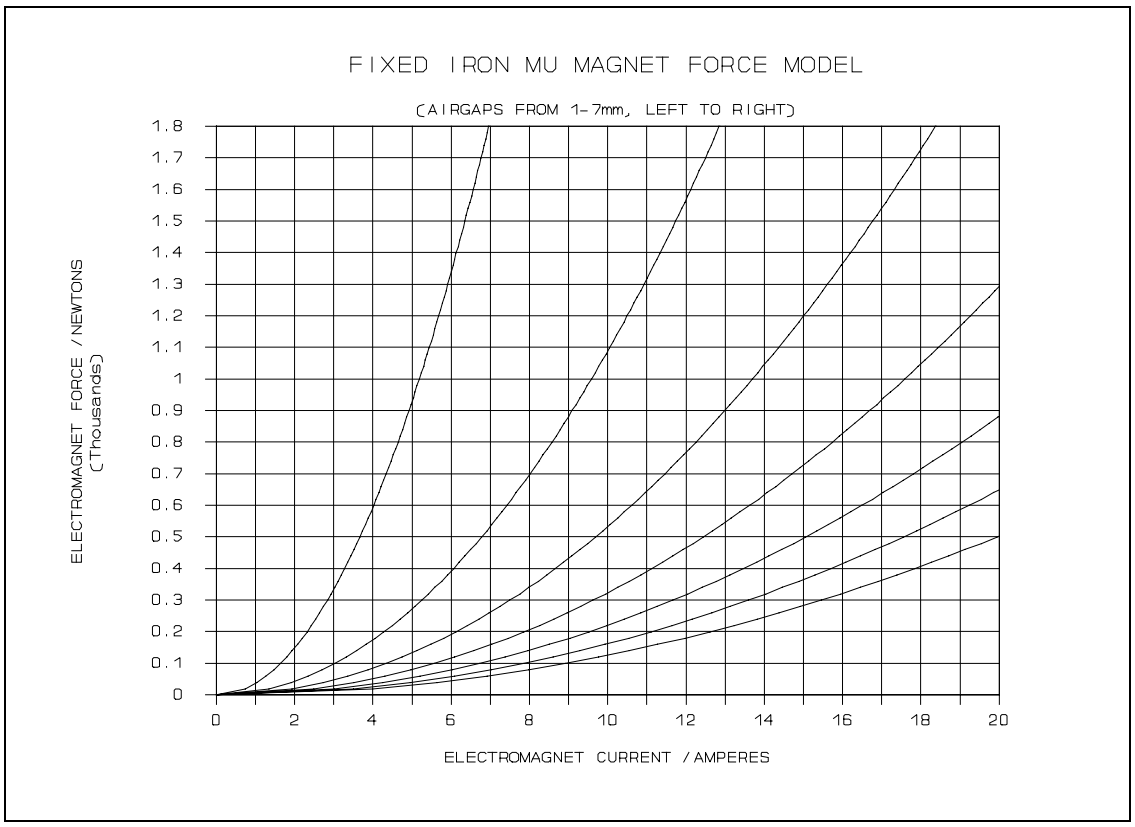

Figure 2.5 Electromagnet lift force model with fixed μ_{iron} (Equation 2.20)

Equation 2.9 due to the effects of the iron path reluctance, and leakage flux. The lift force is reduced by 4% at an air gap of 1 mm and by 11% at 7 mm.

Figure 2.6 shows a graph of the full model of the electromagnet lift force predicted by Equation 2.20 with the iron path permeability dependent on the iron flux density according to the values given in Table 2.2. This graph illustrates the effect of the fall in the permeability of the electromagnet core as it approaches saturation. It also shows clearly the effect of increased leakage flux at larger air gaps, which causes reduced maximum lift force due to the electromagnet core saturation.

2.3.7 Accuracy of the steady-state model

The steady-state characteristics of the electromagnet have been analysed and model equations have been developed. The lateral force of the electromagnet will not be controlled by the suspension control system and therefore the quality of the lateral force model is not investigated in this work. However, to verify the accuracy of the lift force model equations, a simple electromagnet controller was implemented to permit accurate experimental measurements. Experimental data has been obtained by measuring the

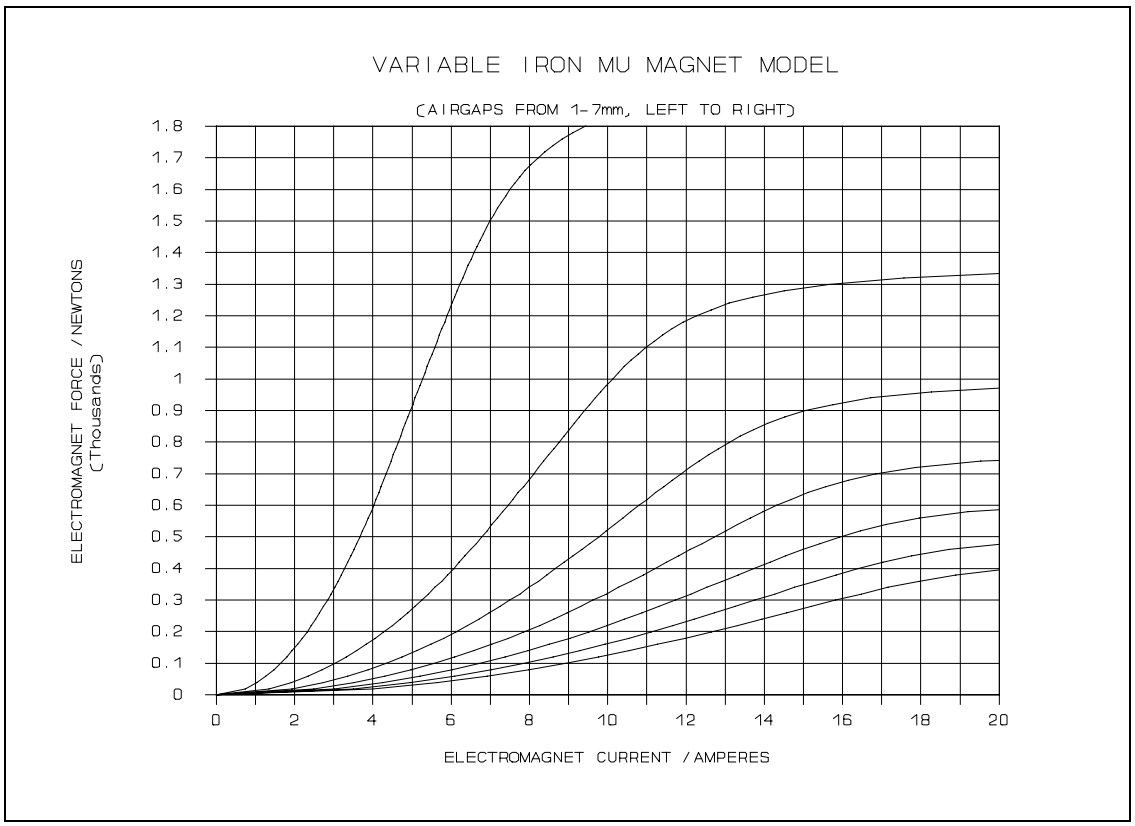

Figure 2.6 Electromagnet lift force model with variable μ_{iron} (Equation 2.20)

electromagnet current whilst suspending a range of different loads at various suspension air gaps. Figure 2.7 shows a graph of the predicted lift force (from Equation 2.20) along with the measured data from the experimental electromagnet which are plotted as diamonds. The uncertainty of each experimental data point due to measurement error is represented approximately by the area of the diamond markers.

Magnetic hysteresis within the electromagnet and track cores causes the experimental current measurements to vary by approximately ±5%, ±1½% and ±1% at air gaps of 1 mm, 3 mm and 5 mm respectively. To isolate this effect from the underlying steady-state force characteristic, the experimental values plotted in Figure 2.7 are the mean of measurements taken with both a rising and a falling flux level.

The performance of the air gap fringe flux model is evident at low forces, before the onset of core flux saturation. The model accuracy is very good for air gaps of 1-4 mm, and then steadily deteriorates as the air gap to pole width ratio exceeds about ½. At higher flux densities, when the core reluctance becomes significant even at large air gaps, the overall model accuracy remains good. The force model error ranges from -2½% to +7% for air gaps up to 5 mm, and then increases to a maximum of about +9% and +13% at air gaps of 6 mm and 7 mm respectively.

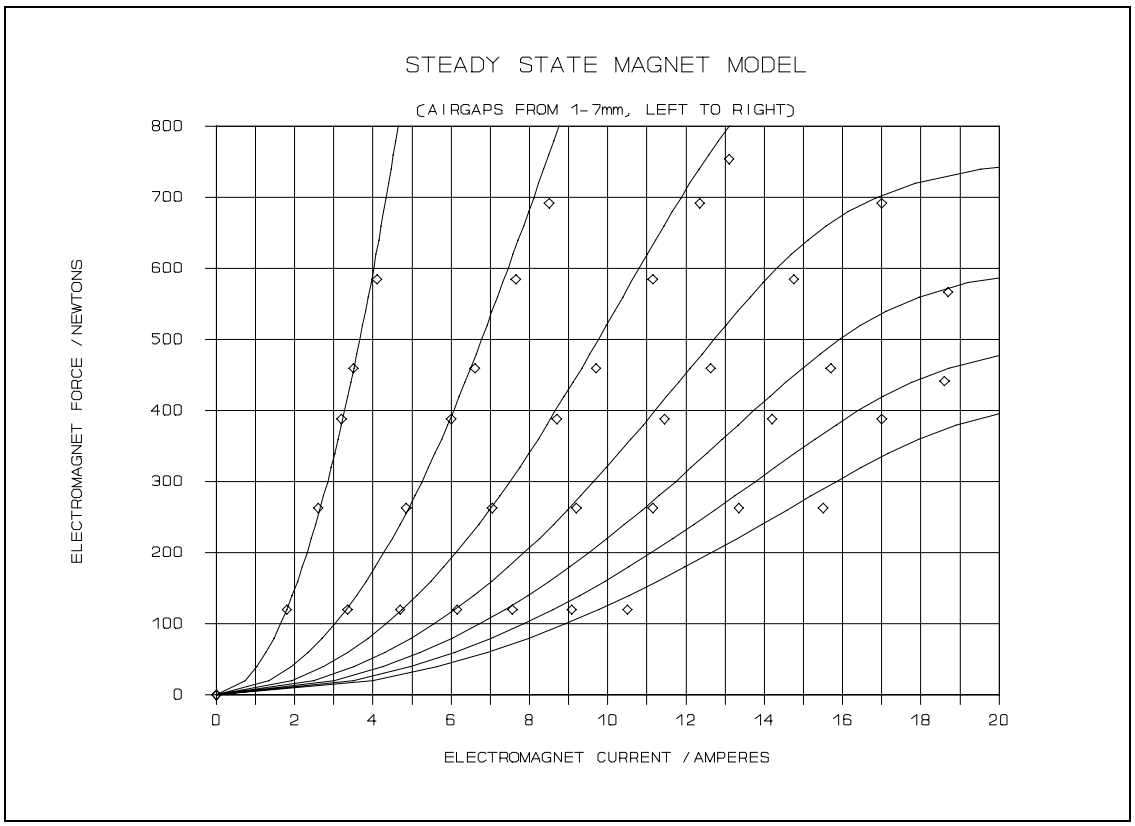

Figure 2.7 Steady state lift force model (Equation 2.20) and measured values.

2.4 Dynamic analysis

The models developed so far have dealt with the steady-state characteristics of the electromagnet. Analysis of the dynamic characteristics is also required because the open-loop instability of the electromagnet necessitates the use of closed-loop feedback control. The dynamic relationship between force and flux is considered first. This is followed by models of the flux and coil current dynamics. Eddy current effects are then modelled and finally, the effect of magnetic hysteresis is discussed.

2.4.1 Magnetic force

The instantaneous force exerted between the electromagnet and its track can be approximated as a function of air gap flux Φ_{airgap}, by using Equations 2.4, 2.5 and 2.7 to give:

$$F_{magnet} = \frac{\Phi_{airgap}^2}{\mu_o A_{pole}} \qquad newtons \qquad \textbf{2.25}$$

The predicted leakage flux between the electromagnet poles varies from being less than the air gap flux at small suspension air gaps to being larger than the air gap flux at the maximum air gap. This effect is significant because even for a constant force, the electromagnet core flux must double as the air gap varies from minimum to maximum. Since a change of core flux is required both for changes in force and changes in suspension air gap length, the dynamics of the flux circuit must now be considered.

2.4.2 Magnetic flux

The relationship between electromagnet core flux Φ_{magnet}, applied coil terminal voltage V and coil current I, is given by:

$$V = N \frac{d\Phi_{magnet}}{dt} + I R_{coils} \qquad volts \qquad \textbf{2.26}$$

where N is the number of coil turns and R_{coils} is the total coil resistance.

Equation 2.26 is useful for dimensioning the voltage requirement of the power controller for the electromagnet. The maximum supply voltage needed is the sum of the parasitic voltage needed for the maximum steady state current requirement plus the voltage needed to provide the maximum required flux slew rate.

The dynamic behaviour of the electromagnet current must now be considered to determine the time constant associated with changes in applied coil terminal voltage, current, flux and air gap.

2.4.3 Coil current

A first order approximation to the electromagnet flux, Φ'_{magnet}, can be obtained by substituting Equations 2.6 and 2.7 into Equation 2.4, giving:

$$\Phi'_{magnet} = \frac{\mu_o A_{pole} NI}{2g} \qquad webers \qquad \textbf{2.27}$$

where N is the total number of coil turns, A_{pole} is the pole face area and g is the suspension air gap length. Substituting Equation 2.27 into Equation 2.26 gives:

$$V = \frac{d}{dt}\left(IL'_{coils}\right) + IR_{coils} \qquad volts \qquad \textbf{2.28}$$

where L'_{coils} is an approximation to the self inductance of the coils which is given by:

$$L'_{coils} = \frac{\mu_o N^2 A_{pole}}{2g} \qquad henrys \qquad \textbf{2.29}$$

The response of Equation 2.28 to a step change in applied coil terminal voltage (assuming constant air gap and hence coil inductance), is given by:

$$I = \frac{V}{R_{coils}}\left(1 - e^{-t/T_{coils}}\right) \qquad amperes \qquad \textbf{2.30}$$

where the electrical time constant T_{coils} is given by:

$$T_{coils} = \frac{L_{coils}}{R_{coils}} \qquad seconds \qquad \textbf{2.31}$$

Equations 2.30 and 2.31 show that the electromagnet coil current experiences a first order lag characteristic relative to the applied terminal voltage. The current lag time constant given by Equation 2.31 also approximates the flux lag time constant due to the coil for changes in applied coil terminal voltage or air gap (see Equation 2.27).

A more accurate model of the coil inductance can be obtained by using Equation 2.24 for Φ_{magnet} instead of Equation 2.27 which gives:

$$L_{coils} = N^2 \frac{R_{track} + 2R_{airgap} + R_{leakage}}{(R_{track} + 2R_{airgap})(R_{leakage} + R_{magnet}) + R_{magnet}R_{leakage}} \qquad henrys \qquad 2.32$$

This expression varies with air gap and core flux density. Table 2.3 lists the predicted inductance (Equation 2.32) and the consequent lag time constant (Equation 2.31) for a range of air gaps, but for a constant iron path permeability.

Table 2.3 illustrates how the leakage flux increases the electromagnet flux (Equation 2.27) at larger air gaps, preventing the inductance from falling as the inverse of air gap (Equation 2.29). The finite inductance at zero air gap is due to the finite permeability of the iron paths. This inductance is an overestimate because the mechanical joints in the iron circuit have been neglected. The table clearly shows that

as the air gap is reduced, the time constant associated with coil current and electromagnet flux is increased.

Table 2.3 Predicted coil inductance and time constant

Air gap	Model L_{coils}	Model T_{coils}
0 mm	1440 mH	1800 ms
1 mm	108 mH	135 ms
2 mm	69 mH	86 ms
3 mm	56 mH	70 ms
4 mm	50 mH	62 ms
5 mm	47 mH	59 ms
6 mm	45 mH	56 ms
7 mm	44 mH	55 ms

2.4.4 Eddy currents

The inductance of the electromagnet coils has been modelled and it has been shown that there is a phase lag characteristic between a change of terminal voltage or air gap and the consequent change of flux. Changes in flux level also generate electro-motive forces in the electromagnet and track cores which cause eddy currents to circulate within the cores. The eddy currents generate a magneto-motive force which opposes the flux change. The resistivity of the core material ensures that the eddy currents decay, so the flux is subject to a lag characteristic. Analysis of the eddy currents is complicated by the distributed nature of the eddy current circuits, each of which encloses only a limited portion of the total core flux.

Yamamura and Ito[42] performed a sophisticated frequency domain analysis of the temporal and spatial effects of eddy currents on core flux. Their analysis produced a model which predicted a first order flux lag with a time constant which increases from the periphery of the core towards its centre. This spatial flux distribution is due to the presence of more effective ‘enclosing turns’ around the centre of the core compared to

the periphery of the core. However, the model required to assist in the synthesis of a control algorithm for the electromagnet does not require a spatial flux distribution model. A novel time domain analysis is therefore proposed which produces a temporal model without a spatial model.

The time domain analysis is performed by considering elemental core circuits, which are then translated to equivalent external coil circuits, ie. coil circuits located outside the core. The external circuits are equivalent to the internal circuits in terms of their total core flux coupling. The contributions of each equivalent external circuit are then combined to give the total flux lag characteristic for a given core geometry. This analysis, for long, thin pole cross sections, is described in Appendix A and results in a first order flux lag model with a time constant given by:

$$T_{eddy} = \frac{\mu_o l_c p^2}{24 \rho g} \qquad seconds \qquad 2.33$$

where p is the electromagnet pole width, l_c is the length of the iron flux circuit, g is the suspension air gap and ρ is the resistivity of the core material. To simplify the analysis, this model neglects the core reluctance, air gap flux fringing and leakage flux. The temporal component of the model proposed by Yamamura and Ito makes the same simplifying assumptions and gives a very similar time constant. The only difference lies in the denominator coefficient which for the frequency domain analysis is $2\pi^2$ versus 24 for the time domain analysis. The frequency domain approach therefore predicts a time constant which is 22% larger than that predicted by the time domain analysis.

Flux lag due to eddy currents appears in two distinct guises. The first is a reaction to variation of the flux level in the electromagnet and track due to changing airgap or changing coil magneto-motive force. For this case, the iron circuit includes both the electromagnet and the track. To improve the accuracy of the model, a correction factor is applied to model the effects of air gap flux fringing (see Equation 2.11), and leakage flux (see Equation 2.15). The effect of leakage flux is modelled by adding it to the suspension flux passing through the track. The time constants predicted by the model are shown in Table 2.4 for a range of air gaps.

The second cause of eddy currents is due to the motion of an electromagnet along its track. Even though the magneto-motive force and air gap are constant, the motion of the electromagnet is continuously magnetising fresh track at the front of the electromagnet. A similar effect occurs at the trailing end of the electromagnet as the

Table 2.4 Predicted eddy current lag time constant for the electromagnet and track

Air gap	Eqn 2.33 T_{eddy}	Leakage & fringe flux correction	Model T_{eddy}
1 mm	11.7 ms	1.36	15.8 ms
2 mm	5.9 ms	1.73	10.2 ms
3 mm	3.9 ms	2.09	8.1 ms
4 mm	2.9 ms	2.46	7.1 ms
5 mm	2.4 ms	2.82	6.8 ms
6 mm	2.0 ms	3.18	6.4 ms
7 mm	1.7 ms	3.54	6.0 ms

track is demagnetised. The flux lag due to the eddy currents reduces the suspension force and generates a drag force which retards the motion of the electromagnet.[43,44] The iron circuit length for the model (Equation 2.33) is in this case just the track flux path length. To improve the accuracy of the model, a correction factor is again applied to model the effects of air gap flux fringing (see Equation 2.11). The time constants predicted by the model are given in Table 2.5.

Due to the motion of an electromagnetically suspended vehicle along its guideway, the track flux lag characteristic appears spatially along the length of the electromagnet. The speed at which the electromagnet length corresponds to 1 flux lag time constant represents a breakpoint above which a significant loss of suspension force occurs. The predicted eddy current lag time constant for the track is 3.5 ms at an air gap of 1 mm (see Table 2.5). This gives a speed break point of 57 m/s for the experimental electromagnet which is 0.2 m long. Since the experimental track for the research vehicle is only 5 metres long, the consequent low maximum vehicle speed prevents this effect from being observed.

2.4.5 Magnetic hysteresis

The magnetisation characteristic for the electromagnet and track steel cores includes significant magnetic hysteresis.[45] Therefore, in addition to the iron permeability being a nonlinear function of flux density, it is also a nonlinear function of flux history.

Table 2.5 Predicted flux lag time constant due to eddy currents in the track core

Air gap	Eqn 2.33 track T_{eddy}	Fringe flux correction	Model track T_{eddy}
1 mm	3.31 ms	1.07	3.53 ms
2 mm	1.65 ms	1.13	1.87 ms
3 mm	1.10 ms	1.20	1.32 ms
4 mm	0.83 ms	1.28	1.06 ms
5 mm	0.66 ms	1.34	0.88 ms
6 mm	0.55 ms	1.40	0.77 ms
7 mm	0.47 ms	1.47	0.69 ms

Since hysteresis affects the core permeability and hence the core reluctance, it is an effect which increases in significance at smaller air gaps. There are very few references to hysteresis in the published literature on electromagnetic suspension control, but Limbert et al[46] referred to doubling the damping feedback gain of their suspension controller to overcome problems which they attributed to hysteresis. Magnetic hysteresis is very difficult to model analytically with even moderate accuracy because of its nonlinear dependence on the history of the core flux.

The steady-state model error caused by the iron core hysteresis increases for smaller air gaps as described in Section 2.3.7. However, due to the small size of the model error for air gaps greater than 2 mm, and the difficulty of modelling hysteresis, the design of the suspension control system is to proceed without the aid of an analytical model for magnetic hysteresis.

Finally, annealing[47] the electromagnet core to relieve the stresses built up during manufacturing increases the iron core permeability and significantly reduces the hysteresis envelope for minimal cost. This reduces the detrimental effects of both hysteresis and iron core reluctance prior to saturation for the experimental electromagnets.

2.4.6 Accuracy of the dynamic model

The flux lags associated with changes in both air gap and applied coil terminal voltage have been modelled. The flux lag time constant is a function of both the coil resistance, which is temperature dependent, and most significantly the inductance, which is a function of air gap. Eddy currents generated within the cores also cause a flux lag characteristic. Both the coil and the eddy current circuits are magnetically coupled to the core with little leakage inductance. The combined effect is therefore modelled by a first-order flux lag (see Appendix A) with a time constant equal to the sum of the coil and eddy current time constants.

The quality of the flux lag model is now tested by comparing the model predictions with experimental measurements from the electromagnet and track. All of the measured flux responses exhibited a dominantly first order lag characteristic.

The electromagnet coil time constant was determined by applying voltage steps to the coil and measuring the flux rise time constant using a Hall plate flux probe and a storage oscilloscope. The measured flux time constant includes a lag contribution from both the coil and the eddy current circuits. The eddy current time constant is therefore subtracted from the measured value to give the coil time constant. The accuracy of the coil time constant is insensitive to errors in the measured eddy current time constant because of the large relative size difference. Table 2.6 lists the model predictions and experimentally measured values for the electromagnet time constant for a range of air gaps.

Table 2.6 Predicted and experimental electromagnet coil time constants

Air gap	Model T_{coil}	Experimental T_{coil}	Error factor
1 mm	135 ms	111 ms	1.21
4 mm	62 ms	76 ms	0.82
7 mm	55 ms	68 ms	0.81

The error between the predicted and measured electromagnet coil time constants ranges from around +20% to -20%. With a measurement accuracy of about ±5% the model

accuracy is seen to be quite satisfactory. This model relies heavily on the static model equations thus giving additional confidence in their accuracy. The error at 1 mm is in part due to an overestimate of leakage flux which is inherent in the static force model equations (see Section 2.3.5). The discrepancies that exist suggest that the iron permeability may be lower than assumed and that the leakage flux may be slightly larger than modelled for large air gaps.

In order to measure the eddy current time constant, the effective coil circuit time constant was significantly reduced. This was achieved through the use of a closed-loop controller incorporating high gain (x 100) current feedback. Analysis of this closed-loop configuration (see Appendix B) shows that current feedback reduces the effective coil time constant, whilst leaving the eddy current time constant unaltered.

Step changes in coil current reference were input to the controller and the flux change time constant was again measured using a Hall plate flux probe and a storage oscilloscope. The measured flux time constant now includes the eddy current lag time constant plus 1% of the coil circuit time constant. The contribution of the coil circuit is therefore subtracted from the measured time constant to give the eddy current time constant. The relative size of the two components gives an eddy current time constant error approximately equal to the measurement error plus one third of the coil time constant error. Table 2.7 lists the predicted and measured values for the eddy current time constant for the electromagnet and track cores over a range of air gaps.

Table 2.7 Predicted and experimental eddy current lag time constants for the electromagnet and track

Air gap	Model T_{eddy}	Experimental T_{eddy}	Error factor
1 mm	15.8 ms	4.6 ms	3.4 x
4 mm	7.1 ms	2.4 ms	3.0 x
7 mm	6.0 ms	1.8 ms	3.3 x

The predicted values are all about 3 to 3.5 times the experimental values. The rather large discrepancy between the model and the experimental system is attributed mostly to the model assumption of uniform core flux distribution and zero core reluctance. In

reality, the flux lag is composed of spatially distributed components, with time constants which are small near the perimeter of the core, but which increase towards the centre of the core. The interaction between distributed flux components is further complicated by the effects of the core permeability.

In addition to the above factors, the model parameters represent an additional error source. All of the core dimensions were measured with high accuracy, however, the core resistivity could not be measured with available equipment. Manufacturing records for the cores do not exist, but they appear to be made of mild steel. If, however, the cores are made of magnetic steel with even as little as 0.5% Silicon content, then the resistivity would be approximately double that of mild steel.[48] In view of the uncertainty associated with the core resistivity, and the otherwise good fit of the first order lag model, further experimental work with a known core resistivity would be required to determine the exact accuracy of the eddy current model time constant.

For the purposes of developing an electromagnet control algorithm, the quality of the first order lag model is considered to be sufficiently accurate when combined with the measured time constants.

It is assumed that if the track cores are made of the same material as the electromagnet cores, then the predicted eddy current time constants for the track alone (see Table 2.5) are also approximately three times too large.

2.5 Concluding remarks

Models have been developed for the significant steady-state and dynamic characteristics of the experimental suspension electromagnet. The force between the electromagnet and its reaction rail is dominantly a function of the core dimensions, the square power of the coil current-turns and the inverse square power of the length of the suspension air gap. The resulting negative stiffness makes the electromagnet open-loop unstable.

The operational envelope for a given electromagnet geometry depends on the maximum achievable air gap flux. This is determined by the flux saturation level of the cores, and the air gap which determines the reduction of air gap flux due to the significant flux leakage between the electromagnet pole pieces. Finite core permeability at low flux levels is also significant for small air gaps. The electromagnet steady-state model equations therefore incorporate variable core permeability and leakage flux.

The dynamic characteristics of the electromagnet force are dominated by the dynamic behaviour of the electromagnet coil current and the eddy currents within the cores. These are a function of the coil inductance and resistance, the core dimensions and resistivity, and the suspension air gap and core permeability. In addition to the electromagnet core flux varying with force, the flux also varies with air gap (at constant force) due to leakage flux varying with air gap. The dynamic behaviour of the electromagnet flux is modelled by a first order lag with a time constant given by the sum of the coil and eddy current time constants.

The accuracy of the steady-state model equations is very good. The characteristic behaviour of the dynamic model equations is also good, but the predicted time constant for the eddy current lag is about 3 times that of the measured time constant. This discrepancy may be largely due to an erroneous estimate for the core resistivity. However, further experimentation with a material of known resistivity is required to validate the model time constant more fully.